Cost-efficient characterization of the aeroacoustic performance of micro-perforated wall-treatments in a wind tunnel

Cédric Maury, Teresa Bravo, Daniel Mazzoni, M Amielh, Laurence Pietri

▶ **To cite this version:**

Cédric Maury, Teresa Bravo, Daniel Mazzoni, M Amielh, Laurence Pietri. Cost-efficient characterization of the aeroacoustic performance of micro-perforated wall-treatments in a wind tunnel. 179th Meeting of the Acoustical Society of America, Dec 2020, Acoustics Virtually Everywhere, France. hal-03430599

HAL Id: hal-03430599
https://hal.science/hal-03430599

Submitted on 16 Nov 2021

HAL is a multi-disciplinary open access archive for the deposit and dissemination of scientific research documents, whether they are published or not. The documents may come from teaching and research institutions in France or abroad, or from public or private research centers.

L'archive ouverte pluridisciplinaire **HAL**, est destinée au dépôt et à la diffusion de documents scientifiques de niveau recherche, publiés ou non, émanant des établissements d'enseignement et de recherche français ou étrangers, des laboratoires publics ou privés.

Cost-efficient characterization of the aeroacoustic performance of micro-perforated wall-treatments in a wind tunnel

Cedric Maury, Ecole Centrale Marseille (LMA), 13013, FRANCE
cedric.maury@centrale-marseille.fr

Teresa Bravo, Consejo Superior de Investigaciones Cientificas (ITEFI), Madrid, 28006, SPAIN
teresa.bravo@csic.es

Daniel Mazzoni, Muriel Amielh and Laurence Pietri, Aix Marseille Université, Marseille, Provence-Alpes-Côte d'Azur, 13013, FRANCE
daniel.mazzoni@centrale-marseille.fr
amielh@irphe.univ-mrs.fr
pietri@irphe.univ-mrs.fr

1.INTRODUCTION

Reduction of flow-induced noise constitutes a line of continuous research as acoustic standards are formulated considering more stringent criteria as well as further integrated end-user and eco-friendly factors. For instance, Turbulent Boundary Layer (TBL) constitutes a broadband noise source for an aircraft under cruise conditions that contributes to cabin noise between 500 Hz and 2 kHz.[1-3] Although passive methods may add additional weight and are accompanied by some degradation in high-lift / low-drag performance, they continue to be developed due to their straight realizations in practical applications. Overall, low frequencies, which are predominantly transmitted, are difficult to control without the introduction of massive components. Acoustic liners, when optimized, are efficient to reduce noise propagation in low-speed flow ducts such as in exhaust silencers[4] or in high-speed flow ducts such as at the inlet of aircraft turbofans.[5] Their acoustic and aerodynamic properties in presence of grazing flow opens up several questions, especially how to maintain high dissipation performance while keeping low skin friction.[6]

These dissipative wall treatments are typically made of perforated sheets rigidly-backed by an air cavity, a honey-comb core, or filled with porous or fibrous materials. Structures composed of micro-perforated panels (MPPs) have become an alternative solution to porous materials since they can be used in hostile environments[7] and do not introduce added mass. These devices are resonance absorbers composed of a panel with sub-millimetric holes backed by a cavity.[8,9] Optimal performance are achieved by a proper selection of the panel thickness, of the size and shape of the perforations, of the perforation ratio (or porosity) and of the cavity depth. The goals are to increase the viscous losses through the apertures that dissipate the acoustic energy around the Helmholtz resonance, and to obtain high absorption values over a broad bandwidth. The advantages come from the fact that they are light compact devices that can be fitted in the small spaces available, for instance within sidewalls. They can easily be

cleaned and maintained, are not flammable and can be manufactured with materials having tailored properties.

Locally-reacting wall treatments are typically made up of micro-perforated sheets backed by a cellular honeycomb core. Such devices are Helmholtz-type narrowband resonators that can significantly dissipate noise at mid-frequencies.[8] Their dissipation is induced either by visco-thermal losses within the holes or by acoustically-induced vorticity at the holes inlet/outlet. Their input impedance can be optimized to ensure efficient attenuation of the least attenuated duct mode,[10] typically the planar mode. On the other hand, bulk-reacting wall treatments, easier to manufacture, occur when the MPP-shielded cavity is filled with a material that enables wave propagation along directions within the cavity that are tangential to the MPP surface. This can be an air cavity or a cavity filled with large fibre radius anisotropic materials.[11,12] Bulk-reacting liners typically exhibit a broader attenuation bandwidth than the locally-reacting ones, although with lower values of the maximum attenuation.[13]

Careful design of such acoustic treatments requires a suitable characterization of their attenuation properties in presence of grazing flow. This can be achieved through flow duct experiments using either direct measurements of the liner input impedance through the moving microphone or the two microphones techniques.[14] In the former, a sample of the resistive layer under test, for instance a MPP, is placed on a rigid-walled cavity. The set is flush mounted onto a flow duct wall, the material being submitted to an acoustic plane wave at grazing incidence. Sound pressure is measured at two positions: one at the sample surface and one at the rear wall of the cavity. The probe is placed on a motorized micrometric displacement system. It crosses the cavity and the duct flow domains, measuring acoustic pressure from the rear wall of the cavity to the opposite side of the duct. For that, two holes should be drilled perpendicular to the probe axis crossing the MPP surface for microphone positioning. Also, the probe calibration is difficult and dependent on the flow characteristics. Measurements disturbances make this intrusive methodology subject to error that led to use the two microphones technique, where one microphone is flush mounted at the surface of the layer and another is flush mounted at the rear of the cavity. During the calibration phase, both microphones are placed at the rear of the cavity, where the pressure field is uniform. By measuring the transfer function between the microphones, they are calibrated one in comparison with the other. It is then a non-intrusive technique for the flow, but destructive for the MPP. Moreover, these very small microphones are little sensitive and very fragile.

Another direct method is based on Laser Doppler Velocimetry (LDV) measurements[15,16] that estimate the acoustic velocity components extracted from the fluctuating velocity field nearby the liner surface through a decorrelation technique. This technique enables aeroacoustic measurements in a noninvasive way and with a fine spatial resolution. However, it requires delicate expensive instrumentation as well as particle seeding of the flow which may obstruct the MPP holes.

The aim of this work is to compare the ability of a number of micro-perforated resonant absorbers (MPRA) and fibrous non-resonant absorbers (NRA) to attenuate flow-induced and acoustically-induced pressure levels measured in a low-speed wind tunnel within and out of the turbulent boundary layer. A constraint was to use cost-efficient measurement techniques such as nosecone microphones, albeit intrusive. The following sections are summarized as follows. Section 2 will furnish a general description of the experimental test-bench consisting of a wind tunnel and the two types of samples used in this work. We will also characterize the TBL developed over the devices to be tested. Section 3 provides a complete description of the performance of the resonant and non-resonant absorbers to reduce the flow-induced noise and the acoustically-induced noise by a set of structured measurements for a constant flow speed. The reduction ability for both flow-induced and acoustically-induced noise, will be assessed from sound pressure level (SPL) spectra measurements performed with the nosecone microphones. The paper will finish with the main conclusions and some indications for further research.

2.EXPERIMENTAL SET-UP

A.SAMPLES DESCRIPTION

A photograph of two micro-perforated samples, tested sequentially under the same conditions is presented in Fig. 1.

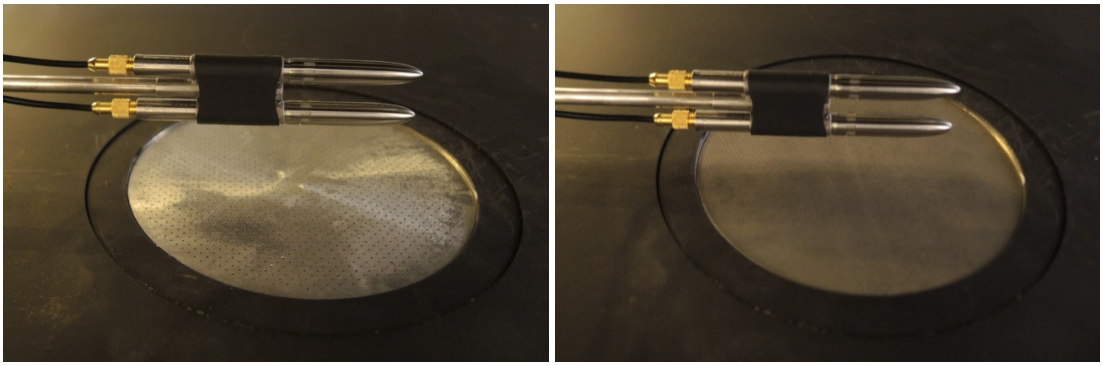

Figure 1. Photograph of the micro-perforated absorbers: MPRA1 (left) and MPRA2 (right)

The physical constitutive parameters characterizing the two MPPs are summarized in Table 1. As it can be seen, the most important difference appears in the holes separation distance that determines the perforation ratio, with classical values for the MPRA1, around 3%, but a much higher porosity for MPRA2, almost 80%, that can be classified as an ultra-microperforated panel.

Table 1. Constitutive parameters of the two MPRAs samples

Panel sample	Holes diameter (mm)	Holes pitch (mm)	Porosity (%)	Thickness (mm)
MPRA1	0.5	2.5	3.14	0.5
MPRA2	0.2	0.2	78.54	0.2

The second class of materials that will be compared with the resonant absorbers are presented in Fig. 2. In this case, the air cavity is filled with two different fibrous materials, NRA1 composed of vertical plastic fibers and NRA2 composed of twisted sisal fibers.

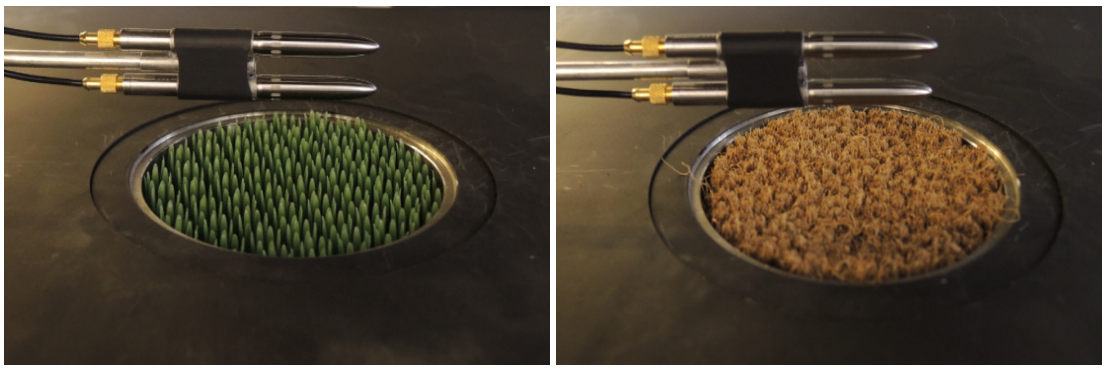

Figure 2. Photograph of the fibrous absorbers: NRA1 (left) and NRA2 (right)

The behavior of these four samples will be tested experimentally in situations where both turbulent and acoustic excitations coexist.

B.WIND TUNNEL EXPERIMENTS

The overall experimental facility is shown in Fig. 3. Experiments have been performed in the Eiffel-type wind-tunnel of the IRPHE Fluid Dynamics Laboratory in order to assess the effects of MPRAs wall-treatments on the sound field in presence of a low-speed TBL of air. The test section of the closed-loop wind-tunnel is 5 m long and has a square cross-section equal to $0.44\,\mathrm{m}\times 0.56\,\mathrm{m}$. Several silencers are located upstream and downstream the fan section. An even airflow is accelerated through a convergent from a settling chamber equipped with honeycomb straighteners. A sandpaper strip was fixed spanwise

3m upstream the test panel in order to efficiently trig the airflow transition to turbulence so that a fully-developed turbulent flow was established at the axial position where the samples are flush-mounted.

Figure 3. Overall view of the IRPHE low-speed wind-tunnel facility

Acoustic excitation has also been generated by the installation of a compression driver flush-mounted on the lateral walls of the wind tunnel, 2 m upstream of the test section. As it can be seen in Fig. 4, it is a BMS 4591 compression driver, efficient over the frequency range 200 Hz – 9 kHz.

Figure 4. Photography of the acoustic compression driver mounted on the wind tunnel wall

Fig. 5 shows the cylindrical cavity of depth 30 mm and diameter 94 mm to position the different specimens to be flush-mounted on the sample section. A millimetric hole has been drilled at the centre of the cavity floor to enable sound pressure measurement using a pinhole microprobe GRAS 40SC, used for decorrelation of the signals.

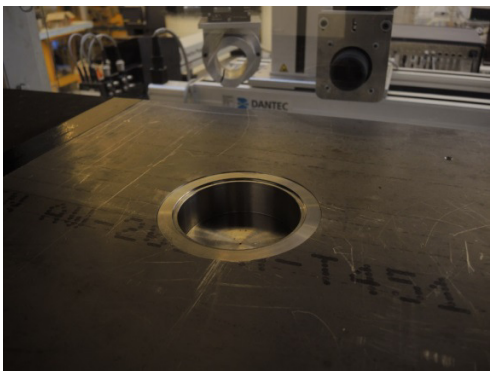

Figure 5. Cylindrical cavity to position the different flush-mounted samples

Fig. 6 shows how one of the samples is flush-mounted on the cavity situated on the floor of the wind-tunnel measurement section. We could also appreciate the pair of nosecone microphone that acquire acoustic pressure above the sample. The outer shape of the RA0022 forebody surrounding each ¼" microphone cartridge has been optimized to ensure low self-noise and a stable stagnation point at the nosecone tip.[17] Prior calibration of the nosecone microphones ensured a correction factor lower than 1 dB on their sensitivity below 4 kHz for incidence angles varying between 0° and 90° with respect to their axes.

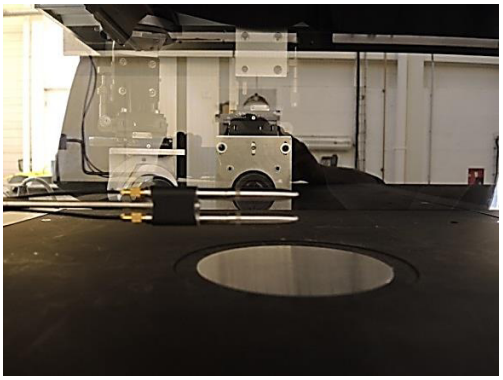

Figure 6. Picture of a plain panel flush-mounted on the base wall of the wind-tunnel test section

A representation of the measurement positions using the pair of nosecone microphones is outlined in Fig. 7. Both nosecone tips are fixed by a support and located 13 mm apart from each other and the microphone pair position can be displaced step-by-step along the horizontal and vertical directions using a motorized system. Up to 5 horizontal positions, equally spaced along the diameter of the specimens, and 12 vertical positions, were measured under a constant flow velocity. This provides a total number of 24 positions along the vertical line over the samples as two nosecone microphones measurements can be acquired for each vertical location.

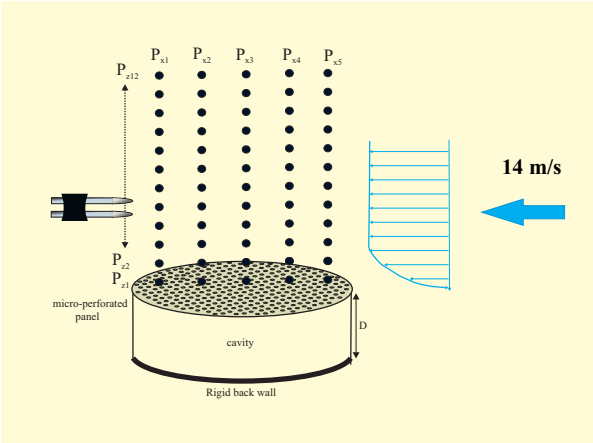

Figure 7. Schematic of the different measurement positions along the horizontal and vertical directions over the test sample

C.AERODYNAMIC MEASUREMENTS

Prior aerodynamic measurements have been carried out at $14\,\mathrm{m\,s^{-1}}$ to characterize the TBL fully-developed over the different samples. A calibrated X-hot film probe has been used to measure the mean and fluctuating parts of the horizontal and vertical flow velocity components. The vertical separation distance z from the samples surfaces has been sequentially monitored to obtain the horizontal and vertical velocity profiles. The measurements have been performed denser close to the flush-mounted

surface, within the TBL thickness, and more spaced out of the TBL. Results on the mean velocity profiles are shown in Fig. 8 and 9 for the resonant and non-resonant absorbers, respectively.

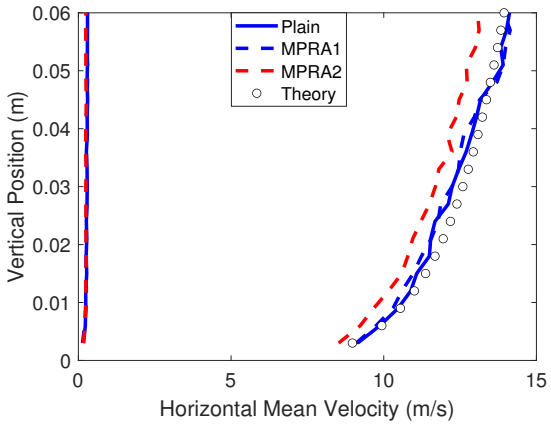

Figure 8. Mean-flow velocity profiles for the horizontal (right) and vertical (left) components above a plain panel (solid blue), the MPRA1 (dashed blue) and the MPRA2 (dashed red) samples. The universal law for the mean velocity profile is also presented (black circles)

It can be seen that the vertical mean flow component along z, U_z, is almost constant (around $0.24\,\mathrm{m\,s^{-1}}$) and much lower than the TBL grazing mean flow component along x, U_x, as could be expected. The TBL measured over a plain panel, in blue, closely follows the universal seventh power law of z/δ, namely $U_x(z)=U_\infty(z/\delta)^{1/6.8}$ with $\delta=0.071\mathrm{m}$ the TBL boundary layer thickness obtained from the grazing flow Reynolds number $\mathrm{Re}_x=x_0U_\infty/\upsilon$ as $\delta=0.38x_0\,\mathrm{Re}_x^{-1/5}$ with $x_0=3.82\,\mathrm{m}$ the separation distance between the probe and the boundary layer trigger point and $\upsilon=1.5710^{-5}\,\mathrm{m^2\,s^{-1}}$ the air kinematic viscosity at 20°C. When comparing this universal law with the velocity profiles of the resonant absorbers (Fig. 8), it can be seen that the curves are very similar for MPRA1, with no significant differences with the plain panel. The situation is different for the highly porous MPRA2 resonant absorber. In this case, experimental values of U_z systematically underestimate the universal TBL velocity profile above a smooth panel by 10%. This is accompanied by a decrease of the skin friction velocity from $u_\tau=0.55\mathrm{m\,s^{-1}}$ over the smooth floor down to $u_\tau=0.31\mathrm{m\,s^{-1}}$ over MPRA2, estimated from a fit of the measured data to the logarithmic region of the boundary layer. These effects could be due to the high density of holes for the ultra-microperforated panel.

Fig. 9 shows that flow measurements over the fibrous absorbers lead to an underestimate by 5% of the universal TBL velocity profile. It could be hypothesized that, as it was the case for the ultra-microperforated panel, this defect of axial mean velocity might be due to vertical transport of flow momentum across the highly porous surfaces MPRA2, NRA1 and NRA2.

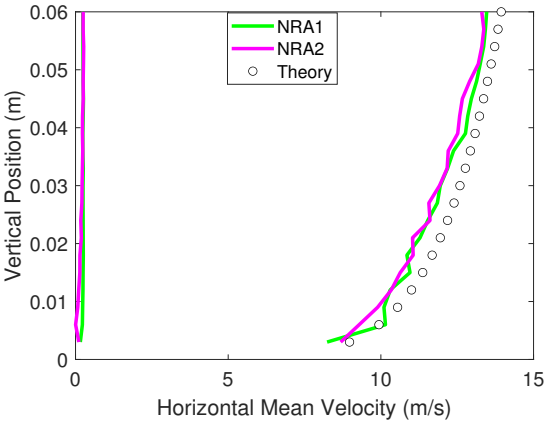

Figure 9. Mean-flow velocity profiles for the horizontal (right) and vertical (left) components above the NRA1 (green) and the NRA2 (magenta) samples. The universal law for the mean velocity profile is also presented (black circles)

3.CONTROL OF FLOW-INDUCED NOISE

A.ATTENUATION OF FLOW INDUCED NOISE

The performance of the resonant and fibrous absorbers for the reduction of flow-induced noise will be analyzed in this section, starting for control of pure flow noise in the wind tunnel test section. Measured results for the MPRAs are shown in Figs. 10 and 11, that present the sound pressure levels (SPLs) spectra measured at a particular position, $z = 3\,\text{mm}$, above the surface specimen, and the profiles over the vertical direction for different frequencies, respectively. The nosecone microphones have been displaced from 3 mm to 72 mm to properly cover the extension of the TBL thickness, that has been determined as $\delta = 0.071\,\text{m}$. Interchanging the plain panel by the MPRA1 resonant absorber provides a flow-induced attenuation with a maximum value of 5.5 dB at 3 KHz. The control bandwidth extends from 1300 Hz to 4300 Hz. The corresponding values for the highly-porous MPRA2 comprise a maximum attenuation of 7.5 dB at 3 kHz and a control frequency band that starts at a higher frequency, from 1600 Hz to 3.5 kHz. These characteristics can be analyzed more in detail from the complete vertical profile shown in Fig. 11. At low frequencies below 400 Hz, both MPRAs present very poor attenuation results, and start to be performant when increasing the frequency above 1000 Hz. Both MPRAs are then efficient over a zone that extends up to 40 mm above the panels under test. In general, the attenuation zone is rather localized in the vicinity of the wall treatment since it does not exceed 20 mm above 2 kHz, and a larger surface treatment would be required to extend it.

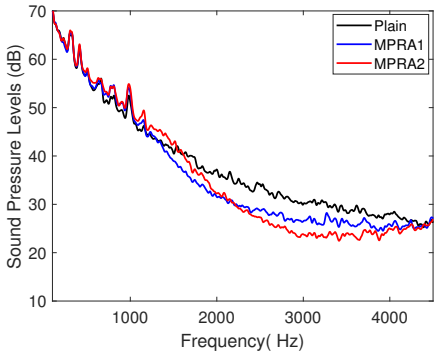

Figure 10. SPLs measurements of the attenuation of flow-induced noise at $z = 3\,\text{mm}$ above the plain floor (black), MPRA1 (blue) and MPRA2 (red)

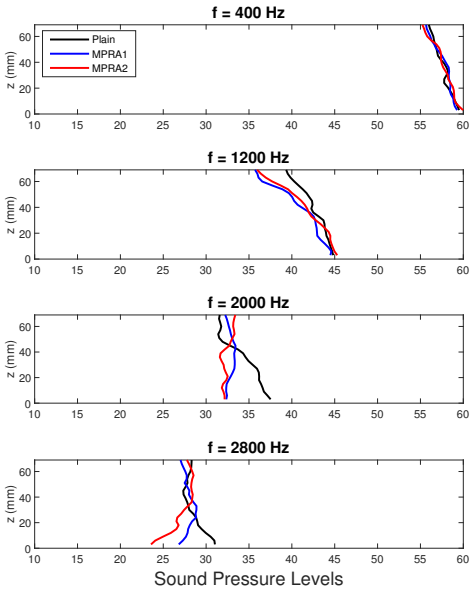

Figure 11. Measured SPL profiles along a vertical axis above the plain floor (black), MPRA1 (blue) and MPRA2 (red) at different frequencies of analysis

When interchanging the resonant absorbers by the fibrous samples, we can appreciate that the performance are clearly diminished both on maximum values and attenuation bandwidths. Inserting the twisted sisal into the cylindrical cavity, leads to a flow-induced noise reduction by up to 5.3 dB at 2.7 kHz. At this frequency, both NRAs are able to provide attenuation over a zone of 40 mm above the flush-mounted surface, similar to those provided by the MPRAs.

Generally, NRA2 is more efficient than NRA1 to reduce flow-induced noise due to its ability to dissipate the wall-pressure fluctuations through the micro-channels bounded by the sisal fibers with a tortuosity greater than one. A unit tortuosity and a denser array of fibers in NRA1 could explain its lower efficiency to reduce flow-induced noise.

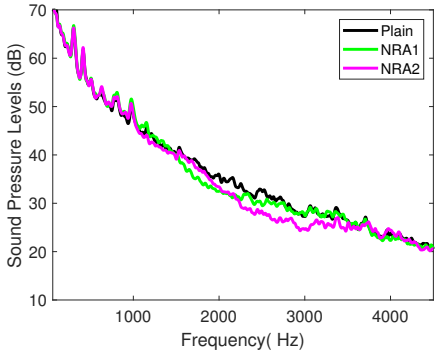

Figure 12. SPLs measurements of the attenuation of flow-induced noise at $z = 3\,\mathrm{mm}$ ***above the plain floor (black), NRA1 (green) and NRA2 (magenta)***

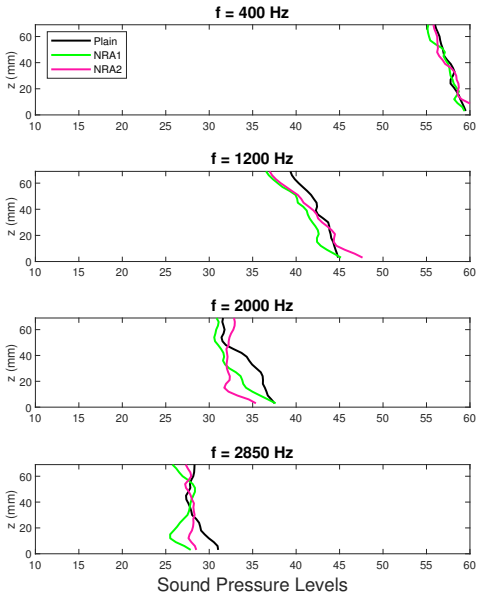

Figure 13. Measured SPL profiles along the vertical axis above the plain floor (black), NRA1 (green) and NRA2 (magenta) at different frequencies of analysis

B.ATTENUATION OF SOURCE INDUCED NOISE

The compression driver presented in Fig. 4 has been flush-mounted on one lateral wall of the wind tunnel, 2 m upstream the test section. It was driven by a white noise signal over a bandwidth between 200 Hz up to 9 kHz to test the ability of the different samples to reduce the acoustic pressures in presence of the TBL flow described in the previous subsection. To remove the effect of the TBL pressure fluctuations over the SPL measurements, a decorrelation technique has been used that provides the following cross-spectral density for the acoustic pressure signals, $S_{\tilde{p}\tilde{p}} = \left|S_{pu}\right|^2 / S_{uu}$, with p the measured pressure signal and u the acoustic source drive signal. This filtering of pseudo-noise induced up to 12 dB decrease of the pressure averaged spectra below 300 Hz.

Fig. 14 compares the SPLs measured at 3 mm over the mounted panel surfaces for the resonant absorbers. It shows that the classical MPRA1 achieves a maximum attenuation value of 14 dB at 1800 Hz, extending the efficiency bandwidth between 1300 Hz and 3200 Hz. The ultra-microperforated MPRA2 performs better, reducing noise up to a maximum of 21 dB at 2600 Hz, albeit at a higher frequency than MPRA1, from 1800 Hz to 3.6 kHz. The absorber performance can also be analyzed along the vertical SPL profiles plotted at different frequencies. As before, due to the limited size of the materials, the attenuation area extends above a limited zone of 40 mm over the different surfaces. Increasing the frequency of analysis, the resonant absorbers are not able to provide attenuation for the source-induced noise in presence of the flow above 3600 Hz.

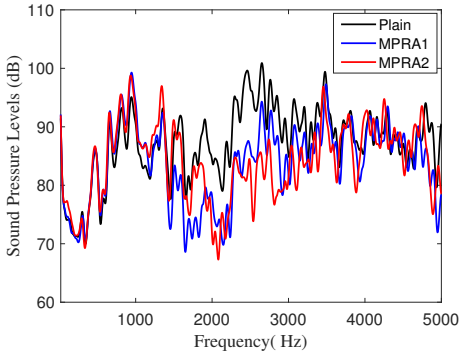

Figure 14. SPLs measurements of the attenuation of acoustically-induced noise at $z = 3\,\mathrm{mm}$ ***above the plain floor (black), MPRA1 (blue) and MPRA2 (red)***

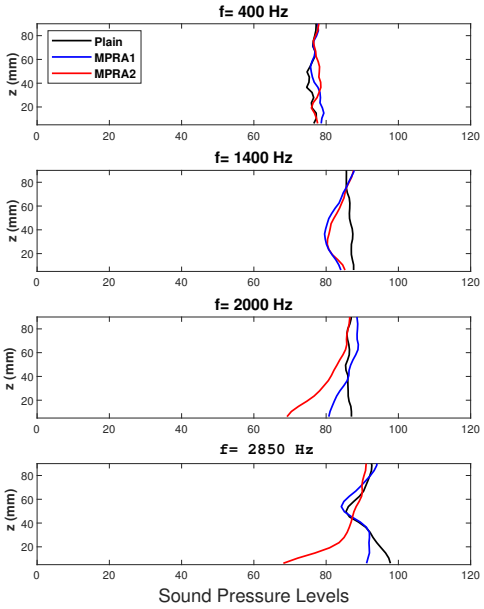

Figure 15. Measured SPL profiles along the vertical axis above the plain floor (black), MPRA1 (blue) and MPRA2 (red) at different frequencies of analysis

Performing similar measurements for the non-resonant samples, Figs. 16 and 17 confirm that NRA1 with vertical plastic fibers performs better than NRA2 with twisted sisal fibers. NRA1 is able to reduce acoustically-induced noise by up to 18 dB between 1500 Hz and 3 kHz as well as another bandwidth around 4500 Hz whereas NRA2 achieves up to 14 dB noise reduction between 2500 Hz and 3800 Hz. Over these frequency bands, the normal impedance over the surface of the fibrous absorber contributes to attenuate the duct modes excited by the upstream source that propagate though the flow duct test section.

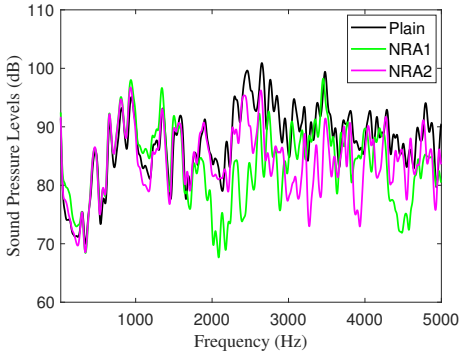

Figure 16. SPLs measurements of the attenuation of acoustically-induced noise at $z = 3\,\mathrm{mm}$ above the plain floor (black), NRA1 (green) and NRA2 (magenta)

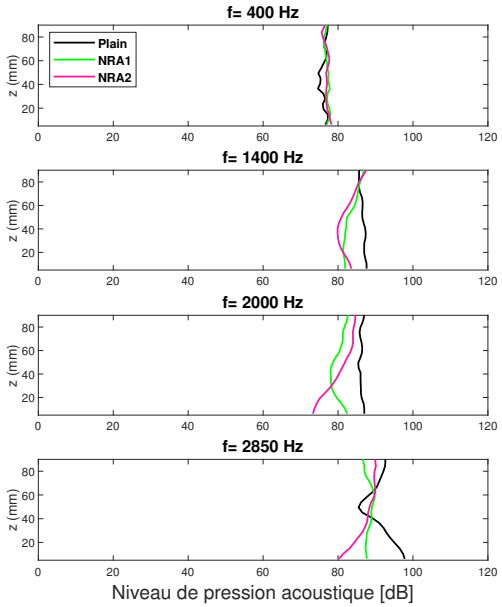

Figure 17. Measured SPL profiles along the vertical axis above the plain floor (black), NRA1 (green) and NRA2 (magenta) at different frequencies of analysis

Finally, Fig. 18 shows the vertical component of the acoustic intensity in close proximity to the flush-mounted surfaces of all the materials tested. The plain smooth panel SPL profiles have been compared against those of the resonant absorbers (MPRA1 and MPRA2) and of the non-resonant absorbers (NRA1 and NRA2) at 2 kHz for the reduction of the acoustically-induced noise in presence of a mean flow at $14\,\mathrm{m\,s^{-1}}$. Estimation of the acoustic intensity in a flow has been done under the assumption that flow effects can be neglected for estimating the peak values of the acoustic velocity spectrum.[18,19]

The analysis of the intensity components for the plain disk shows that the vertical intensity component close to the surface is almost null, as it could be expected in order to satisfy the Neumann boundary condition. Compared with the resonant absorbers MPRA1 and MPRA2, a substantial change in the acoustic behavior can be clearly appreciated at this frequency through an important decrease of the tangential intensity component. This zone of attenuation extends up to 90 mm above the flush-mounted micro-perforated surfaces. As it has been shown before, the highly porous MPRA2 presents a better performance, providing almost a vertical intensity component distribution.

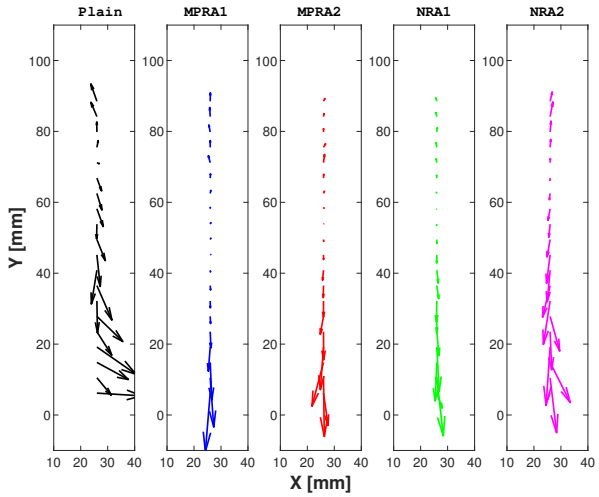

Figure 18. Variations of acoustic intensity profiles measured at 2 kHz in the wind tunnel test section along a vertical line above the axis of the plain panel (black), MPRA1 (blue), MPRA2 (red), NRA1 (green) and NRA2 (magenta).

As it was the case for MPRA1 and MPRA2, the acoustic intensity vector above the non-resonant absorbers NRA1 and NRA2 is also directed towards the porous surface of the absorber. This leads to a noticeable vertical flux of acoustical energy that occurs, here at 2 kHz, within the bandwidth of efficiency of MPRA1, MPRA2 and NRA1, and with a lower efficiency for NRA2 since an axial component of energy is also observed on the rightest figure.

4.CONCLUSIONS

In this work, we have studied the ability of micro-perforated and fibrous absorber for the reduction of pure flow-induced and acoustically-induced noise in presence of a mean flow using cost-efficient nosecone microphones in the experimental test bench. This is an alternative to other techniques either destructive (two-microphones method) or not widely available such as the LDV. It has been found that resonators covered by micro-perforated panels are more efficient than fibrous absorbers to reduce the pure flow-induced noise over a broader bandwidth and with higher attenuation levels. Both MPP resonators and fibrous absorbers provide a greater level of attenuation for the sound pressures induced by an acoustic source than by the flow although over a more restricted bandwidth. Measurements of the acoustic intensity point out a vertical flux of energy towards the surface of the MPP resonators and of the absorbers.

Continuation of this research will be carried out through numerical Lattice Boltzmann simulations to better understand the attenuation mechanisms above the absorbers. This work will also be directed towards the set-up of experimental measurements by hot wire anemometry for the estimation of the attenuation properties of the tested materials under acoustic excitations.

ACKNOWLEDGMENTS

This study was funded in Spain by the Ministerio de Economía y Competitividad project TRA2017-87978-R, AEI/FEDER, UE, and the mobility program ILINK+2018. It was supported in France by the programme A*MIDEX Excellence Initiative of Aix-Marseille University in the framework of the LabeX Mechanics and Complexity AAP2 and by the ANR VIRTECH (ANR-CE10-0012-01). The authors would like to thank A. Ouaked (Master student) for the source-induced measurements.

REFERENCES

[1] G.M Corcos, “The resolution of pressures in turbulence”, Journal of the Acoustical Society of America 35, 192–199 (1963).

[2] A. Caiazzo, R. D’Amico and W. Desmet, “A generalized Corcos model for modeling turbulent boundary layer wall pressure fluctuations,” Journal of Sound and Vibration 372, 192–210 (2016).

[3] A.V. Smol'yakov and V.M. Tkachenko, “Model of a field of pseudosonic turbulent wall pressures and experimental data”, Soviet Physics-Acoustics 37, 627–631 (1991).

[4] S. Allam and M. Åbom, “A new type of muffler based on microperforated tubes”, Journal of Vibration and Acoustics 133, 031005, (2011).

[5] L. Leylekian, M. Lebrun and P. Lempereur, “An overview of aircraft noise reduction technologies”, Aerospace Laboratory Journal 7, AL07-01 (2014).

[6] B.M. Howerton and M.J. Jones, “Acoustic liner drag: measurements on novel facesheet perforate geometries”, in: Proceedings of the 22nd AIAA/CEAS Aeroacoustics Conference, AIAA 2016–2979, Lyon, France, (2016).

[7]H.V. Fuchs and X. Zha, “Micro-perforated Structures as Sound Absorbers – A Review and Outlook”, Acta Acustica united with Acustica 92, 139–146 (2006).

[8] D.Y. Maa, “Microperforated-panel wideband absorbers”, Noise Control Engineering Journal 29, 77–84, (1987).

[9] D.Y. Maa, “Potential of microperforated panel absorbers”, Journal of the Acoustical Society of America 104, 2861–2866 (1988).

[10] R. Kabral, L. Du and M. Åbom, “Optimum sound attenuation in flow ducts based on the "exact" Cremer impedance”, Acta Acustica united with Acustica 102, 851–860 (2016).

[11] T. Bravo and C. Maury, “Sound attenuation and absorption by micro-perforated panels backed by anisotropic fibrous materials: Theoretical and experimental study”, Journal of Sound and Vibration 425, 189–207 (2018).

[12] L.D. Koch, “Investigation of a Bio-inspired Liner Concept”, NASA Technical Document 0005665, NASA Glenn Research Center, Acoustics Branch, (2017).

[13] U. Ingard, Noise Reduction Analysis, Jones and Bartlett Publisher, London, UK, 2010.

[14] C. Malmary, S. Carbonne, Y. Aurégan and V. Pagneux, “Acoustic impedance measurements with grazing flow”, in Proceedings of the 7th AIAA/CEAS Aeroacoustics Conference, AIAA-2001-2193, Maastricht, The Netherlands, (2001).

[15] A. Minotti, F. Simon and F. Gantié, “Characterization of an acoustic liner by means of Laser Doppler Velocimetry in a subsonic flow”, Aerospace Science and Technology, 12 (5), 398-407 (2008).

[16] J.C. Valière, Acoustic Particle Velocity Measurements using Lasers, John Wiley & Sons Publisher, Hoboken, USA, 2014.

[17] T. Dassen, H. Holthusen and M. Beukema, “Design and testing of a low self-noise aerodynamic microphone forebody”, Technical Report NLR TP 96320, National Aerospace Laboratory, Amsterdam, The Netherlands, 1–15 (1996).

[18] F.J. Fahy, “Measurement of sound intensity in low speed turbulent airflow”, Proceedings of Internoise 88, pp. 83–88 (1988).

[19] D.H. Munro and K.U. Ingard, “On Acoustic Intensity Measurements in the Presence of a Mean Flow Sound”, Journal of the Acoustical Society of America 65, 1402–1406 (1979).